Volume 15 | Number 10 | 14 March 2019 | Pages 2105–2302

Soft Matter

rsc.li/soft-matter-journal

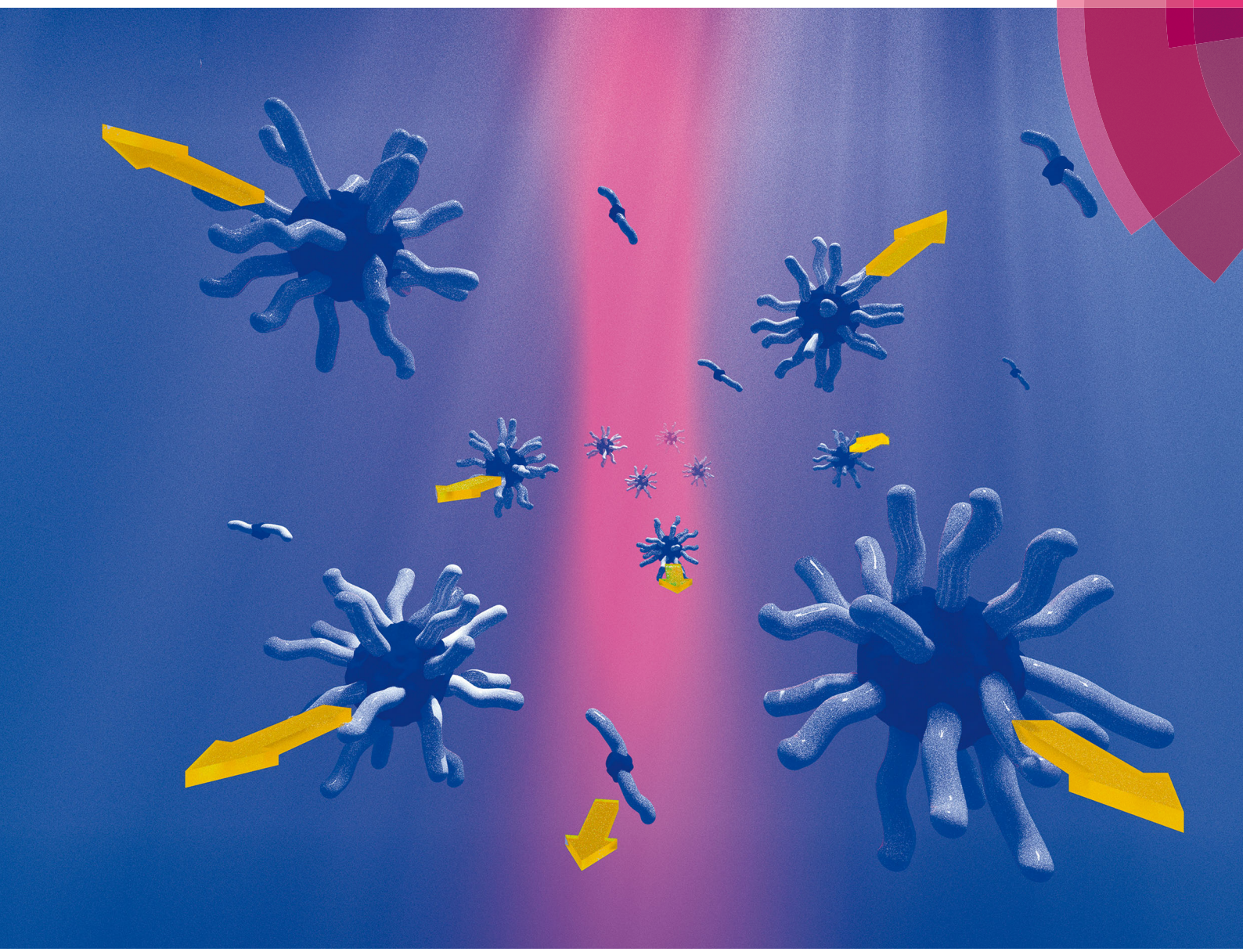

ISSN 1744-6848

ROYAL SOCIETY OF CHEMISTRY | Celebrating IYPT 2019

PAPER
Roberto Piazza *et al.*
Thermophoresis in self-associating systems: probing poloxamer micellization by opto-thermal excitation

Soft Matter

PAPER

View Article Online
View Journal | View Issue

Cite this: *Soft Matter*, 2019, **15**, 2140

Thermophoresis in self-associating systems: probing poloxamer micellization by opto-thermal excitation

Enrico Lattuada, Stefano Buzzaccaro and Roberto Piazza *

Received 23rd November 2018,
Accepted 13th January 2019

DOI: 10.1039/c8sm02386g

rsc.li/soft-matter-journal

Due to its exquisite sensitivity to interfacial properties, thermophoresis, *i.e.*, particle motion driven by thermal gradients, can provide novel, exclusive, and often surprising information on the structural properties of colloidal or macromolecular fluids and on particle/solvent interactions at the nanoscale. Here, by using an all-optical thermal excitation technique, thermal lensing, we show that thermophoresis can be profitably exploited to investigate the self-association of an amphiphilic block copolymer, poloxamer P407, which takes place above a concentration-dependent critical micellization temperature (cmt). In particular we show that, around and above the cmt, the direction of the poloxamer thermophoretic motion displays a remarkable double sign inversion, which is fully correlated with a peak in the thermal expansivity of the solution marking the progressive dehydration of the propylene oxide groups of P407 and their incorporation into the micellar core. This rather puzzling behaviour of the thermophoretic mobility and of the Soret coefficient in the P407 micellization region can tentatively be explained by properly taking into account the temperature-dependent balance between micellized and nonassociated poloxamer chains.

1 Introduction

Particle thermophoresis is a nonequilibrium cross-flow effect between mass and heat transport, akin to thermal diffusion (the Soret effect) in simple fluid mixtures.[1,2] When a colloidal suspension or a macromolecular solution is placed in a temperature gradient, the dispersed particles display, on top of Brownian motion, a steady drift velocity given by $v_T = -D_T\nabla T$, where the thermophoretic mobility D_T is often dubbed the "thermodiffusion coefficient". Then, depending on the sign of D_T, the particles focus either at the cold or the hot side, leading to the steady-state concentration gradient given by $\nabla c = -c(1-c)S_T\nabla T$, where c is the particle mass fraction and $S_T = D_T/D$ is called the Soret coefficient. With this definition, $S_T > 0$ when the particles move to the cold side.

While its phenomenological description in the framework of nonequilibrium thermodynamics is well-established, thermophoresis can conversely be designated as one of the most challenging test cases for statistical mechanics. On the one hand it involves a much plainer situation than those typically addressed by nonequilibrium physics, like those related to large fluctuations, hydrodynamic instabilities, or chaotic motion. Soret motion originates indeed from a very simple condition (a homogeneous two-component fluid in a uniform temperature gradient) and eventually leads to a smooth spatially-inhomogeneous but time-independent state. On the other, however, thermophoresis poses fundamental questions that go to the very heart of the statistical description of nonequilibrium phenomena. For instance, what is the microscopic origin of the phenomenological coupling between heat and mass transport assumed in thermodynamics? May the action of a thermal gradient be represented as the effect of a fictitious 'thermal force' acting on the particles? Can a nonequilibrium stationary state (NESS) be fully described using local equilibrium concepts, as usually assumed in 'standard' nonequilibrium thermodynamics?†

No ultimate answers to these thought-provoking questions have so far been given, hence a fully consistent microscopic description of 'thermal forces' is yet to come. As a matter of fact, the same basic questions affect the development of fully reliable numerical simulation methods for thermally inhomogeneous systems, as evidenced by recent attempts to quantify

CMIC, Dipartimento di Chimica, Materiali e Ingegneria Chimica, Politecnico di Milano, 20133 Milano, Italy. E-mail: roberto.piazza@polimi.it

† An insightful discussion of this question has been given by Sasa and Tasaki.[3] Here we simple recall that a local equilibrium approach cannot account for particle thermophoresis in gases, whose kinetic description necessarily requires one to consider the first correction (proportional to ∇T) to a local Maxwell–Boltzmann distribution.[4] Similarly, van't Hoff's original explanation of the Soret effect,[5] based on assuming a constant local chemical potential, turned out to be totally wrong, since it predicts that any solute has the same Soret coefficient $S_T = 1/T$.

the thermo-osmotic slip of a fluid close to a thermally inhomogeneous wall, an effect strongly related to thermophoresis.[6,7]

Thermophoresis is challenging even within the less fundamental scope of colloidal science.[8,9] Although it bears strong similarities with other kinds of 'phoretic' motion,[10] extensive experimental investigations of thermophoretic effects in colloids, and macromolecular and surfactant solutions have indeed unraveled a much wider scenario than in the case of simpler interfacially-driven phenomena like electrophoresis.

For instance, for a given disperse system in a specified thermodynamic state, it is even extremely hard to predict whether the particles will preferentially move to the cold or to the hot side, namely whether they will show 'thermophobic' ($S_T > 0$) or 'thermophilic' ($S_T < 0$) behaviour. While field-driven effects such as electrophoresis are generally determined by simple particle properties such as surface charge, thermophoresis seems indeed to be sensitive to details of the particle/solvent interfacial interactions. The origin of this delicate sensitivity to interfacial properties is captured by hydrodynamic models,[11,12] which are however too general to provide quantitative predictions for a given system, except in a few specific cases.

Besides, no microscopic model is so far able to properly account for some general and rather puzzling features of thermophoresis. Among them, it is worth mentioning the strong and very peculiar dependence of the Soret coefficient on temperature for aqueous systems.[13] In a nutshell, a large class of colloidal dispersions, and macromolecular, biological, and even simple molecular solutions[14] in water behave as 'thermophobic' at sufficiently high T, but become thermophilic below a system-dependent temperature T^* following a rather universal temperature dependence.

Although still poorly quantifiable, this distinctive dependence on details of the interfacial interactions and on temperature is at the root of a recent boom of applications of thermophoresis to particle trapping and manipulation,[15–17] microscale separation and fractionation,[18,19] highly selective investigation of biomolecular interactions,[20,21] or even to the manipulation of single biomolecules inside a cell.[22]

Here, using an all-optical thermal excitation method, thermal lensing, we plan to show that thermophoresis can give useful and in many senses surprising information on the temperature-driven self aggregation of poloxamers, a class of block copolymers with amphiphilic properties that have extensive biomedical and pharmaceutical applications. Specifically, within the temperature range where self-aggregation of a poloxamer solution takes place:

(i) The Soret coefficient displays a remarkable 'double sign inversion', never reported so far for any investigated system.

(ii) The thermal expansivity of the solutions also shows a pronounced peak that fully correlates with previous calorimetric investigations.

(iii) The time-dependence of thermophoresis, when contrasted with the microscopic Brownian dynamics measured by dynamic light scattering (DLS), displays an unexpected slowing down within the region where the poloxamer self-association takes place.

A semi-quantitative understanding of these rather surprising results requires one to consider a model of thermophoresis for a system displaying a temperature-dependent equilibrium between coexisting species. Such a model suggests that other effective forces, besides those usually assumed to explain thermophoresis, are at work. All together, the results presented in this paper indicate that thermophoresis can be a unique tool to unravel subtle restructuring effects in soft matter systems.

2 Thermal lensing in complex fluids

Thermal lensing (TL) is a self-effect on beam propagation taking place when a laser beam heats up a partially absorbing medium, generating a locally inhomogeneous refractive index profile.[23,24] Thermal expansion induces indeed a local density distribution in the sample that, in its turn, produces a refractive index profile acting as a negative lens that increases the divergence of the transmitted beam.

Consider a Gaussian laser beam of optical power P, incident on a sample of thickness ℓ with absorption coefficient b, thermal conductivity κ, and thermal diffusivity χ, and assume for simplicity a 2-D geometry that neglects heat flow along the optical axis. Then, in the paraxial approximation, the heat equation yields a parabolic local refractive index profile

$$\Delta n(r,t) = -\frac{Pb}{2\kappa}\frac{\partial n}{\partial T}\frac{1}{\pi w^2(1+\tau_{\rm th}/2t)}r^2, \qquad (1)$$

where $\tau_{\rm th} = w^2/4\chi$ is the heat diffusion time over the beam-spot size w. Hence, the sample acts as a simple diverging lens with inverse focal length

$$\frac{1}{f_{\rm th}} = -\vartheta_{\rm th}\frac{\lambda}{\pi w^2(1+\tau_{\rm th}/2t)}, \qquad (2)$$

where we have defined a dimensionless 'thermal lens number'

$$\vartheta_{\rm th} = -\frac{Pb\ell}{\kappa\lambda}\frac{\partial n}{\partial T}, \qquad (3)$$

so that $\vartheta_{\rm th} > 0$ if $\partial n/\partial T < 0$ (like for water at $T \gtrsim 0$ °C).

The TL effect can be accurately measured by focusing the incident beam on the sample with a lens and detecting the time-dependence of the light intensity $I(t)$ at the beam center (namely, on the optical axis) with a photodiode. Let us call $\bar{z} = z_0/z_{\rm R}$ the distance z_0 from the cell to the position of the beam waist (the position, coincident with the geometrical focus of the lens, where the incident beam attains its minimal radius w_0) rescaled to the Rayleigh range $z_{\rm R} = \pi {w_0}^2/\lambda$, which is a measure of the 'depth of focus' of the focusing lens. Then, to first order in $\vartheta_{\rm th}$ (*i.e.*, for weak TL effects) $I(t)$ is given by

$$I(t) = \frac{I(0)}{1+\vartheta_{\rm th} f(t;\tau_{\rm th})}, \qquad (4)$$

where the function

$$f(t;\tau) = \frac{\bar{z}}{\bar{z}^2+3}\frac{\pi}{\sqrt{3}(1+\tau/t)} \qquad (5)$$

is evaluated for $\tau = \tau_{\rm th} = w^2/4\chi$, which is the characteristic heat diffusion time over the beam spot size. This simple expression also takes into account aberrations of the thermal lens with

respect to a simple parabolic approximation and is a very good approximation to an exact 2D Fresnel diffraction analysis.[25] Notice that the intensity change depends not only on ϑ_{th} but also on $\bar{z}$, and is maximal when $\bar{z} = \pm\sqrt{3}$, namely when the cell (assumed to be thin with respect to z_R) is placed at a distance equal to $\sqrt{3}z_R$ from the beam waist (where conversely, at first order in ϑ_{th}, the TL effect vanishes). Placing the cell at this particular position (where the beam size is $w = 2w_0$) we simply have

$$f(t;\tau) = \frac{\pi}{6}\frac{1}{1+\tau/t}. \quad (6)$$

The time-dependence of the TL signal yields therefore a simultaneous measurement of the sample thermal conductivity, thermal diffusivity, and specific heat too, $c_p = \kappa/\rho\chi$.

By inducing the TL effect using high-power laser pulses of short duration, one can also investigate the nonlinear optical properties of complex fluids such as ionic liquids.[26] TL effects are also extensively exploited in analytical chemistry. Indeed, since the TL technique is capable of detecting absorption in simple fluids with extinction coefficients as low as 10^{-7}, it was soon established as a highly sensitive technique for trace analysis in chromatography and electrophoresis, both in its basic configuration and in more sophisticated instrumentation design including double-beam, differential, spectrally-tunable setups.[27,28] It is also worth noticing that, due their sensitivity and high spatial resolution, TL methods naturally lend themselves to microfluidics applications, thermal imaging (TL microscopy), and single-particle detection.[29,30]

Besides its excellent performance as a spectroscopic method, however, TL can be profitably exploited to investigate the Soret effect in fluid mixtures or thermophoresis in colloids. Indeed, the laser-induced temperature profile drives Soret motion, which leads to the progressive buildup of a concentration gradient within the heated region acting as an additional lenslike element. This 'Soret lens' can be divergent or convergent depending on the preferential direction of motion of the component with the largest index of refraction and, as a result, the spreading of the transmitted beam further increases, or conversely lessens. For instance, in a suspensions of particles with a refractive index larger than the solvent, thermophoresis leads to a larger or smaller beam spreading depending on whether S_T is positive or negative.

Eqn (4) is readily extendible to the simultaneous presence of thermal and Soret lensing effects by writing

$$I(t) = \frac{I(0)}{1+\vartheta_{th}f(t;\tau_{th})+\vartheta_S f(t;\tau_S)}, \quad (7)$$

where $\tau_S = w^2/4D$ is the mass diffusion time, with diffusion coefficient D, over the beam spot size and we have defined the 'Soret lens number'

$$\vartheta_S = -\frac{Pb\ell}{\kappa\lambda}\frac{\partial n}{\partial c}S_T c(1-c), \quad (8)$$

where c is the mass concentration of the solute. Notice that, due to the different orders of magnitude of thermal diffusivity and mass diffusion, 'thermal' and 'Soret' lensing effects usually take place on widely separated time scales. Besides, since

$$\frac{\vartheta_S}{\vartheta_{th}} = -S_T c(1-c)\frac{\partial n/\partial c}{\partial n/\partial T}, \quad (9)$$

an independent determination of the temperature and concentration dependence of the refractive index allows one to obtain a differential measurement of the Soret coefficient that neither depends on the thermal conductivity and optical absorbance of the medium, nor on the values chosen for P and ℓ. It is finally convenient to define a time-dependent TL number

$$\vartheta(t) = \frac{6}{\pi}\left(\frac{I(0)}{I(t)}-1\right) = \frac{6}{\pi}[\vartheta_{th}f(t;\tau_{th})+\vartheta_S f(t;\tau_S)], \quad (10)$$

which at large t is easily seen to reach the asymptotic value

$$\vartheta(\infty) = \vartheta_{th}+\vartheta_S = -\frac{Pb\ell}{\kappa\lambda}\left[\frac{\partial n}{\partial T}+\frac{\partial n}{\partial c}S_T c(1-c)\right]. \quad (11)$$

A seminal investigation of the Soret effect in an aniline/cyclohexane mixture close to the critical point[31] showed that TL can be regarded as an all-optical technique combining accuracy in generating localized thermal gradients with experimental simplicity. However, at variance with this strongly absorbing mixture, water is highly transparent throughout the whole visible range. Indeed, water absorption becomes substantial only for wavelengths $\lambda \gtrsim 1.2$ μm, where the quantum efficiency of silicon solid-state photodetectors is unfortunately very low. Moreover, water is surely not an ideal solvent for TL measurements, since at room temperature it has a rather low value of $\partial n/\partial T$, which actually vanishes just below 0 °C.‡ In principle, aqueous colloidal suspensions could be investigated with TL by adding a small amount of a water-soluble dye. Yet, this requires a careful assessment of potential interactions between the dye molecules and the dispersed particles, which is particularly critical when the latter are polymer chains or surfactant micelles.

Substantial TL effects in a convenient near-IR spectral region can however be obtained without introducing any photosensitive probe by exploiting a specific vibrational overtone of water, peaking around $\lambda \simeq 970$ nm§ yielding an absorption coefficient $b \approx 0.55$ cm^{-1}, which is large enough for obtaining good TL signals. This strategy has been originally exploited by Rusconi *et al.*[32] to successfully measure the Soret coefficient and thermophoretic mobility of surfactant solutions and silica colloids. Later, by taking into account the additional information that can be obtained by just analyzing the purely 'thermal' effect, the same group showed that TL allows one to obtain the thermal conductivity of nanofluids without incurring spurious convective effects that formerly led to unjustified claims about an anomalously high value of this quantity.[33]

‡ Notice that this value does not coincide with the temperature ($T \simeq 4$ °C) at which water attains its maximum density. This witnesses a small deviation of $n(p)$ from the prediction of the Lorentz–Lorenz formula discussed in the following.

§ This band is due to a first harmonic of water symmetric OH stretching combined with the fundamental of antisymmetric stretching (which also produces two other much weaker bands at approximately 740 and 840 nm).

A note of caution should nevertheless be raised concerning convective effects on TL measurements of the Soret effect. Since a radially-symmetric excitation beam generates horizontal temperature gradients, TL measurements on the long time scales required for thermophoretic studies may indeed be influenced by weak natural convection effects that unavoidably set in for any value of the incident power. Although this is not the place for an exhaustive discussion of this subtle and often overlooked problem (which is shared by most thermophoretic measurements based on optothermal excitation of fluids), for what follows it is worth recalling the main results of a general theoretical analysis, supported by extensive numerical simulation.[32] Simple hydrodynamic arguments lead to state that the fluid velocity at the onset of convection scales as $U \propto \ell_g^2 \Delta T$, where ℓ_g is the vertical length over which buoyancy acts and ΔT is the maximum induced temperature difference, which, for an optical path length $l \ll z_R$, is given to a good approximation by¶

$$\Delta T \simeq \frac{Pb}{3\kappa}. \tag{12}$$

Note that, for TL at λ = 970 nm in water ($b \simeq 0.55$ cm^{-1}, $\kappa = 0.61$ W m^{-1} K^{-1}), this yields $\Delta T \simeq 0.03$ K mW^{-1}.

Disturbance of the Soret-induced concentration profile will be negligible provided that, over the beam-spot length scale, mass diffusion is much faster than convection, which happens when $\tau_S \ll w/U$.‖ For a given incident power P, convective effects are weaker the smaller is the quantity $w\ell_g^2$ (= $2w_0\ell_g^2$ at $z = \sqrt{3}z_R$). Reducing the beam waist w_0, however, strongly limits the maximum useful optical path l, since z_R decreases as w_0^2. In practice, even using cells with l as small as 100 μm, w_0 cannot be reduced below 10–20 μm. A much better strategy consists of reducing ℓ_g by placing the optical axis of the setup along the vertical, so that ℓ_g coincides with the optical path l of the cell, which can practically be made much smaller than its lateral extension. In this configuration, $w_0 l^2$ is of the order of the illuminated sample volume. Detailed numerical simulations that also take into account the nonnegligible effect of radiation pressure (which has a stabilizing effect when the incident beam is shone from the top of the setup) show that, in this configuration, convective effects are fully negligible when[34]

$$\frac{wU}{4D} \lesssim 0.1 \tag{13}$$

As we shall see, using the setup and experimental conditions detailed in the following section this requirement is reasonably well satisfied for all the measurements discussed in this paper.

¶ It is worth noticing that eqn (12) is actually obtained by numerically solving the full 3-D heat equation, which duly takes into account axial heat transport, since a simple 2-D approximation leads to a spurious logarithmic divergence of ΔT on the optical axis.

‖ Notice that, conversely, neglecting convection effects on the temperature profile requires $\tau_{th} \ll w/U$, a condition that is usually fulfilled even for rather large values of ΔT. Hence the thermal profile remains essentially unchanged even in the presence of consistent convection.

3 Experimental

3.1 Poloxamer 407 (P407)

Poloxamers, also known by the trade names of Pluronics® and Synperonics®, are a class of water-soluble nonionic $EO_xPO_yEO_x$ block copolymers, where EO is ethylene oxide and PO is propylene oxide, which are available in a broad range of molecular weights and PO/EO ratios.[35] Because of the rich self-aggregation properties stemming from their amphiphilic character, and because of their very low toxicity, they find extensive applications in the formulation of biocompatible drug-carriers.[36] What makes poloxamers particularly interesting and useful in applications is the strong effect of temperature on their aggregation state and phase behaviour. Unlike simple surfactants, these compounds undergo self-aggregation processes not only by increasing the polymer concentration (displaying therefore a critical micelle concentration, cmc), but also by increasing the temperature. At low T, indeed, both the poly(ethylene oxide) and, if y is not very large, the poly(propylene oxide) blocks are fully hydrophilic, and hence the poloxamer is soluble as individual chains, or 'unimers'.** By raising T, however, the central poly(propylene oxide) block becomes progressively more hydrophobic until, for T larger than a concentration-dependent 'critical micellar temperature' (cmt), the chains begin to self-organize into globular micelles where each chain presumably takes on the shape of a highly twisted 'hairpin' with the PO groups preferentially embedded into the micellar core and the EO groups forming a hydrated corona.[37] At variance with the sharp cmc transition of common surfactants, which usually takes place in a very narrow concentration range, extensive experimental evidence shows that this self-association process may require a range of up to 10–15 °C to be fully completed, suggesting that the cmt involves several complex restructuring steps.[38] Upon further increases in polymer concentration and temperature, poloxamers may also form several supramicellar structures which include lyotropic mesophases and micellar polycrystals, hence displaying rich and varied phase diagrams.[39]

Among this wide class of 'polymeric surfactants', Poloxamer 407 (P407) has proved to be a very valuable drug delivery system for a number of routes of administration, in particular because, at concentrations larger than about 20% in weight, it forms thermoreversible gel-like phases at physiological temperature (actually micellar polycrystals with a body-centered cubic structure[40]) that have several advantages in terms of ease of application and drug release efficiency.[41] P407 has a molecular weight $M_w \simeq 12\,600$ Da and a nominal composition $EO_{99}PO_{65}EO_{99}$, but it should be noticed that standard synthesis methods yield polymer chains with a polydispersity of about 10% in the number of EO and PO groups, mostly due to the presence of a small fraction of lower molecular weight EO–PO di-block copolymers. Polydispersity is known to affect the phase boundary and the mechanical properties of the gel phase,[42] but has a much weaker

** Sometimes called 'monomers', although in the context of polymers this term can be misleading.

effect on the micellar association properties at lower concentration.[39,43] Consequently, for the purposes of this work (and also because this is the standard compound in applications) we have used a commercial poloxamer (Pluronic® F127, Sigma-Aldrich, batch # SLBR3970V) without attempting any further purification. A mother batch of P407 at a weight fraction of 20% was prepared by slowly dissolving the polymer in MilliQ water under stirring. This mother batch was then homogenized by ultrasonication and diluted to weight fractions of 1, 5, and 10%, which have been investigated in the temperature range 14 °C < T < 35 °C.

For what follows, it is useful to introduce some general features of the phase behaviour and aggregation state of P407. The cmt of P407, as determined by static light scattering, fluorescence, and viscosity measurements, consistently depends on polymer weight fraction c, decreasing rapidly (cmt $\propto \ln c$) from $T \simeq 40$ °C to $T \simeq 24.5$ °C for $c \leq 1\%$, and then quasi-linearly, with a slope of about -0.7 K^{-1}, for larger values of c.[44] Small-angle neutron scattering (SANS) experiments[45] show that, below the cmt, P407 is dispersed as individual chains with a gyration radius of $R_g \simeq 2.2$ nm. Given the (nominal) total number of EO + PO monomers $N = 263$, a monomer size $a \simeq 2$ nm and the known Kuhn length of EO and PO chains, $b \simeq 1$ nm, this value is consistently lower than the value $R_g = \sqrt{Nab/6} \simeq 3$ nm predicted for a Gaussian chain in a good solvent. This evidence led Mortensen and coworkers[45,46] to suggest that the weakly soluble PO blocks may form partially collapsed globules rather than Gaussian coils, so that below the cmt the P407 chains could actually be regarded as 'unimer micelles' with a central partially hydrophobic unit. A combination of SANS, rheological[47] and DLS[40] measurements show that, well above the cmt, P407 forms globular micelles with an aggregation number of about 50 and a hydrodynamic radius $R_H \simeq 11$ nm, constituted of an internal compacted PO core with a radius of about 4.4 nm and of an external corona made of Gaussian EO chains. The structure of the solution in the extended transition range in between the onset of the micellization process (the nominal cmt) and the final state, where all unimers have been incorporated in micelles, is however much less known. In this paper, we plan to show that the P407 micellization process is more involved and surprising than usually expected.

3.2 TL setup and auxiliary measurements

Solid-state laser sources operating around 970 nm are commonly available as pump modules for erbium-doped fiber amplifiers widely used in optical communications. We have used a fiber-Bragg laser module (MTX9P, Multiplex Inc.) operating at 976 nm with a maximum power $P \simeq 120$ mW, coupled to a 2 m-long monomode optical fiber (Corning Flexcore HI1060) ensuring a well-characterized Gaussian beam profile. The spectral stability of the laser emission is further ensured by a Peltier module powered by a PID temperature controller. An achromatic collimator, placed on a precision gimbal mounting, turns the fiber output into a parallel beam, which, before the measurement starts, is blocked by a digital shutter remotely controlled by a PC. When the shutter is opened by the acquisition software, the beam is fed to an achromatic doublet with a focal length $f = 80$ mm, which focuses the beam to a minimum beam spot $w_0 \simeq 30$ μm, corresponding to a Rayleigh range $z_R \simeq 3$ mm.

The sample is placed into a cylindrical cuvette with an internal diameter of 9 mm and an optical path $l = 200$ μm, enclosed in a quartz jacket allowing one to circulate water from a thermostatic bath (Hellma 165QS). The cell is placed on a micrometric mount allowing for accurate translation along the optical axis, which is required to maximize the TL effect. The transmitted beam is collected in the far-field by a fast photodiode placed behind a 100 μm pinhole selecting less than 0.5% of the beam, which can be accurately placed in correspondence to the beam centre by a precision XY-translator. The current signal from the photodiode is then amplified by a wide-band amplifier, sampled at 10 ks/S by a 16-bit acquisition board, and finally recorded by custom-made software.

As discussed in Section 2, to avoid any convection effect the whole setup is placed vertically. Thermophoretic measurements were performed using an incident laser power of about 12.5 mW, ensuring a maximum temperature increase of less than 0.4 °C on the optical axis. For this incident power, numerical simulations yield a convective velocity $U \simeq 0.1$ μm s^{-1}. Hence, according to eqn (13), natural convection effects are expected to be negligible for values of the diffusion coefficient $D \gtrsim 6 \times 10^{-8}$ cm^2 s^{-1}. As a matter of fact, we never detected any effects of convection, which typically show up as oscillations in the detected signal that grow in time, up to acquisition periods as long as 10^3 s. The setup was calibrated using the TL signal for pure water, taking also into account the small dependence of b on T, shown in the inset of Fig. 1.[48] The measured values of the TL signal for water are shown in the body of Fig. 1 as a function of temperature.

Calibration of the concentration and temperature dependence of the refractive index, $\partial n/\partial c$ and $\partial n/\partial T$, was performed with an Abbemat RXA Digital Refractometer (Anton Paar) with a sensitivity $\Delta n = 10^{-5}$. In the following, we shall also refer to static and dynamic light scattering measurements made with a home-made setup equipped with a 70 mW frequency-doubled Nd$^+$ YAG laser operating at 532 nm, a detecting photomultiplier mounted on a goniometer, and a Brookhaven multi-tau correlator. A small-volume (1 ml) cylindrical cell, immersed in a thermostatted index-matching vat, is provided with a custom-designed filling system allowing the cell to be first carefully cleaned by flushing with a large amount of solvent filtered through a 0.2 μm membrane (at least 100 times the cell volume), then emptied through a PTFE capillary tubing without opening the cell lid, and finally filled with the sample flushed through the same membrane filter. We stress that this careful cleaning protocol, which is not common in commercial light scattering setups, is crucial to avoid any residual dust in the scattering volume, which would strongly affect measurements at low concentration or below the cmt.

4 The Soret effect of P407 at micellization

We first qualitatively discuss the TL results obtained for a dilute solution of P407 in water at 1% w/w. Fig. 2, where we plot a

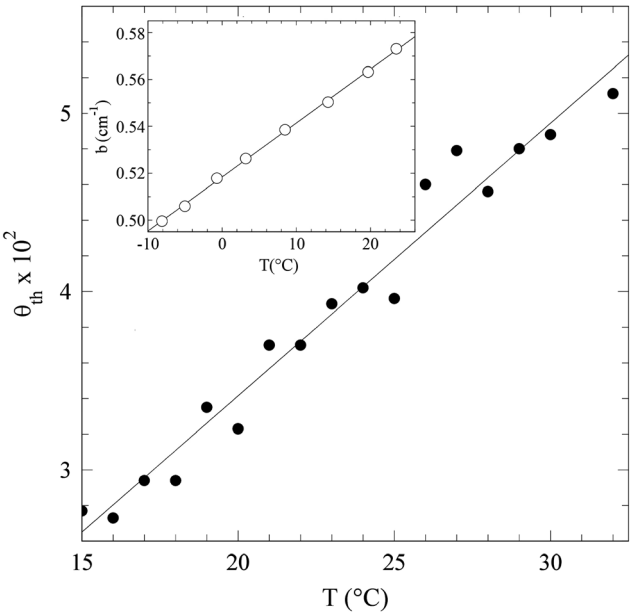

Fig. 1 Temperature dependence of the TL signal ϑ_{th} from pure water, measured with a laser power $P \simeq 22$ mW (corresponding to a temperature increase $\Delta T \lesssim 0.7$ °C on the optical axis). The inset shows the water extinction coefficient $b(T)$ at $\lambda = 975$ nm (see Baptista *et al.* and Tran[48]).

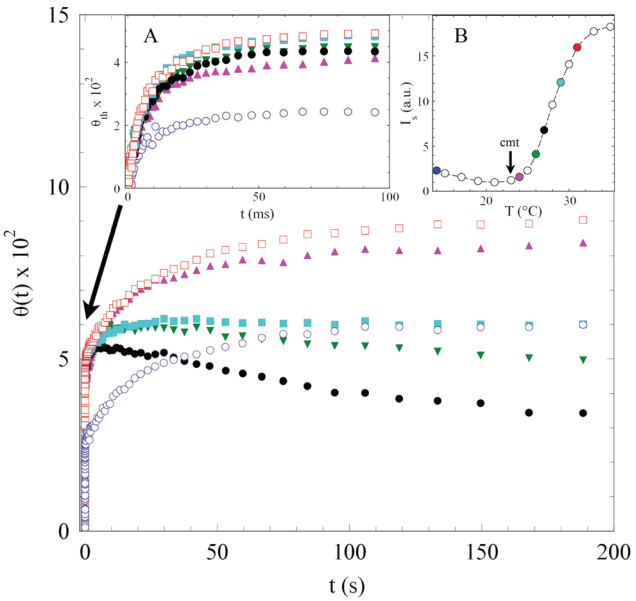

Fig. 2 TL signals for a 1% w/w solution of P407 in water, obtained at 14 °C (open circles), 24 °C (up triangles), 24 °C (down triangles), 27 °C (bullets), 29 °C (full squares), and 31 °C (open squares). The very short-time behaviour of the signals, yielding the thermal lens component, is shown in inset A. Inset B shows the temperature dependence of the scattering intensity, which indicates an increase of the molecular weight by more than one order of magnitude in the temperature range 23 °C $\lesssim T \lesssim$ 35 °C. The full symbols correspond to the temperature values for the signals displayed in the figure body and the arrow indicates the nominal cmt.[49]

selection of the obtained TL signals, highlights a quite unusual temperature dependence. While the short-time trend, shown in inset A, indicates for all values of T a positive value of ϑ_{th} that consistently grows over the whole investigated temperature range, the intensity variation that takes place on much longer time scales due to P407 Soret motion displays a highly non-monotonic behaviour with T. Indeed, the Soret contribution ϑ_S, which is positive at low T, becomes negative for the signals obtained at $T = 26$ °C and $T = 27$ °C, but eventually reverts to a positive value for $T \geq 29$ °C. Inset B, where we plot the intensity of the light scattered at 90°, shows that this anomalous behaviour is fully correlated with the formation of poloxamer micelles.

Quantitative values of ϑ_S can easily be obtained by subtracting from the long-time limit of $\vartheta(t)$ the values of ϑ_{th} obtained from a fit of the short-time behaviour using eqn (2). This allows evaluating from eqn (8) the Soret coefficient S_T, whose temperature dependence, shown by the triangles in Fig. 3, displays a marked negative peak in the range where P407 micellization occurs. Fig. 3 also shows that the values of S_T obtained for P407 solutions at 5% and 10% weight fraction share a very similar behaviour.

This involved 'double switching' from thermophobic to thermophilic behaviour and back in a narrow T-range, which to our knowledge has never been observed so far, seems to be distinctive of the complex mechanisms underlying the temperature-driven self-association of block copolymers, while it is not shared by the micellization of simple surfactants. For instance, let us consider the formation of globular micelles taking place in sodium dodecyl-sulfate (SDS) in the absence of added salts (which may introduce complex thermoelectric effects).[50] The inset in Fig. 3 shows that, by increasing the SDS concentration, the Soret coefficient does show a noticeable increase at the surfactant cmc. Yet S_T remains positive

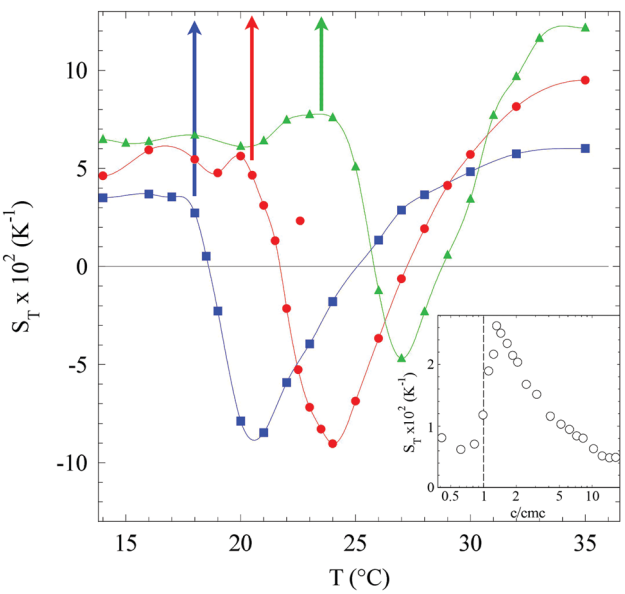

Fig. 3 Body: Temperature dependence of the Soret coefficient for solutions of P407 at a w/w concentration of 1% (triangles), 5% (circles), and 10% (squares). Full lines are just splines to the data. The arrows mark the temperature values where micellization begins. Inset: Soret coefficient *versus* concentration (normalized to the cmc) for SDS solutions.[50]

over the whole concentration range and does not show the peculiar double sign inversion we observed for P407 at the cmt. The latter, whose origin is discussed in what follows, witnesses once again the exquisite sensitivity of thermophoresis to even minimal changes in the interactions between the solvent and the dispersed species.

5 Thermal expansivity at micellization

Inset A in Fig. 2 suggests that the temperature dependence of the purely thermal component ϑ_{th} is conversely rather featureless, and just shows a monotonic increase with T due to the consistent increase of $\partial n/\partial T$ of water in the investigated temperature range. This is not surprising, since at such a low concentration the polymer contribution to the thermal properties of the solution is negligible. However, the experiments performed at higher P407 concentration, shown in the body of Fig. 4, unravel a more complex scenario. Indeed, while for the 1% solution the temperature dependence of $\partial n/\partial T$ is barely distinguishable from that of pure water, at higher concentration the refractive index increment displays an evident negative peak in the same temperature range where we detected the anomalous behaviour of S_T. For comparison, in Fig. 4 we also show the values of $\partial n/\partial T$ for the 5% solution obtained by numerically deriving the refractive index data directly measured by a refractometer, which are in reasonable agreement with the TL data.††

The origin of these peak should be attributed to a non-negligible change in the sensitivity of the solution in the cmt region. For a simple fluid, n is related to the fluid density ρ by the Lorentz–Lorenz equation

$$\frac{n^2-1}{n^2+2} = r\rho \qquad (14)$$

where r is the specific refractivity, namely the optical polarizability per unit mass. This expression, which is the extension at optical frequencies of the Clausius–Mossotti equation for the dielectric polarizability, can be shown to hold also for a colloidal fluid of sufficiently small particles.‡‡ By assuming that r does not appreciably vary in the investigated temperature range and taking the temperature derivative of eqn (14), one easily obtains an expression for the thermal expansivity α of the solution

$$\alpha = -\frac{1}{\rho}\frac{\mathrm{d}\rho}{\mathrm{d}T} = -\frac{6n}{(n^2-1)(n^2+2)}\frac{\partial n}{\partial T}, \qquad (15)$$

which is therefore proportional to $\partial n/\partial T$ *via* a prefactor that, in the investigated temperature range, varies only between 2.71–2.73 for c = 5% and 2.77–2.79 for c = 10%. The specific

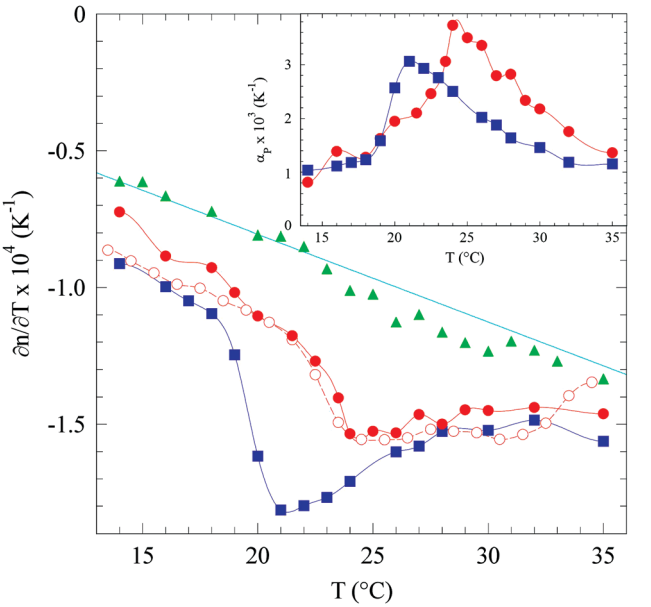

Fig. 4 Body: Temperature dependence of the refractive index increment $\partial n/\partial T$ of P407 solutions at a w/w concentration of 1% (triangles), 5% (circles), and 10% (squares). Full lines are spines to the data to guide the eye. The straight line is a best fit to the values obtained for pure water, which are in excellent agreement with literature data. For comparison, we also show the values of $\partial n/\partial T$ of the 5% P407 solution obtained by a numerical derivative of the refractive index $n(T)$ measured with an Abbemat refractometer. Inset: P407 contribution to the thermal expansivity of the solution obtained from the Lorentz–Lorenz equation as discussed in the text.

contribution α_P of P407 to the thermal expansivity of the solution can therefore be obtained by writing $\alpha = \alpha_P\phi + \alpha_W(1-\phi)$, where ϕ is the volume fraction of the polymer and α_W the thermal expansivity of water. The results, displayed in the inset of Fig. 4, show that P407 undergoes some compaction upon micellization. Notably, this result fully parallels the evidence found using differential scanning calorimetry (DSC) by Wanka *et al.*,[52] who detected a rather strong endothermic peak extending over the whole region where P407 micellization takes place. By carefully analyzing the enthalpy change ΔH associated with this peak for a large number of poloxamer systems, Wanka *et al.* later found that ΔH is directly proportional to the content of PO in the sample. This strongly suggests that the DSC peak is a result of the dehydration of the PO groups, which is in fact the driving force for polaxamer micellization.[39] The close parallel of the calorimetric evidence with that we obtained by analyzing $\vartheta_{th}(t)$ shows that TL can be profitably exploited to unravel and quantify the physical mechanisms leading to self-association.

6 Dynamics and thermophoretic mobility

6.1 Time-dependence of the TL signals

A detailed study of the time-dependence of the TL signals allows us to extract the values of the thermophoretic mobility

†† It is worth noticing that, to minimize computational errors, this measurement requires a fine and accurate temperature scan. In fact, TL, which directly yields $\partial n/\partial T$, proves to be a far more accurate method for measuring the temperature dependence of the refractive index.

‡‡ More precisely, the Lorentz–Lorenz equation holds to order $(\xi/\lambda)^2$, where ξ is the correlation length of the suspension (typically of the order of the particle size) and λ the wavelength of the probing radiation,[51] which is doubtless the case we are considering.

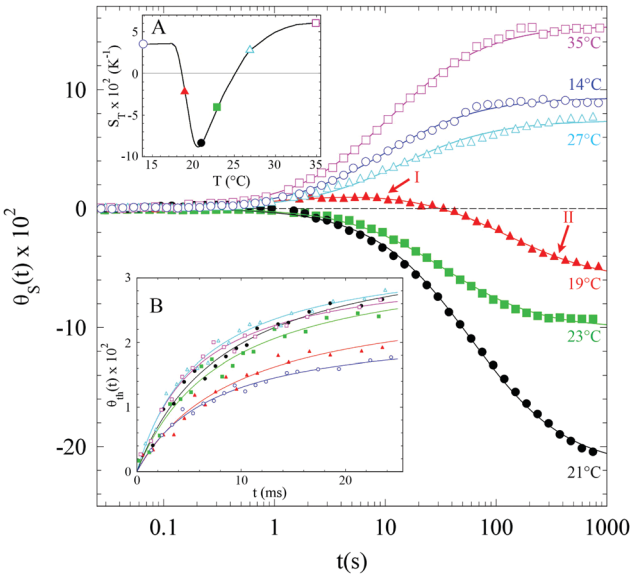

Fig. 5 Body: Time-dependence of the Soret lens number for a 10% w/w P407 solution at particularly telling temperatures (see inset A) obtained from the TL signal $\vartheta(t)$ by subtracting the short-time thermal contribution $\vartheta_{th}(t)$ shown in inset B. The logarithmic time axis emphasizes the occurrence in the signal obtained at T = 19 °C of an initial thermophobic trend (I) followed by a slightly stronger but much slower long-time thermophilic behaviour. Full lines are fits to the data as described in the text.

D_T and, besides, provides novel information about the complex thermophoretic behaviour of P407 solutions in the micellization region. Fig. 5 shows some of the results obtained for a 10% w/w P407 solution at values of T that span the entire investigated temperature range and, as shown in inset A, are representative of the different regimes evidenced for S_T. Picking up the possible occurrence of distinct contributions to the thermophoretic dynamics is visually easier if we first subtract out the purely thermal contribution $\vartheta_{th}(t)$, fitted according to eqn (6) as shown in inset B, and then plot the Soret contribution $\vartheta_S(t)$ on a logarithmic time scale. The figure body shows that all the transients are very well fitted by the simple relaxation function $f(t;\tau_S)$, with the noticeable exception of the curve obtained at T = 19 °C. At this temperature, which lies on the steeply decreasing part of the peak of the Soret coefficient just above the value $T^* \simeq 18.5$ °C where S_T switches from positive to negative, $\vartheta_S(t)$ shows indeed a weak initial increase (region I), followed by a decrease occurring on much longer time scales (region II) that eventually leads to a decidedly thermophilic behaviour. Such a more complex relaxation can nevertheless be nicely fitted by a simple extension of eqn (6) to a situation in which two independent thermodiffusing species are present,

$$f\left(t;\tau_S^s,\tau_S^l\right) = \frac{\pi}{6}\left(\frac{1}{1+\tau_S^s/t}+\frac{1}{1+\tau_S^l/t}\right), \qquad (16)$$

where the relaxation times τ_S^s and τ_S^l are respectively associated to the faster and to the slower diffusing species. For the signal at T = 19 °C one finds $\tau_S^s \simeq 1.25$ s and $\tau_S^l \simeq 130$ s, corresponding to the associated diffusion coefficients $D_s \simeq 7.2 \times 10^{-6}$ cm^2 s^{-1} and $D_l \simeq 6.9 \times 10^{-8}$ cm^2 s^{-1}. It is worth noticing that, while D_s is roughly compatible with the diffusion coefficient of an object the size of a unimer diffusing over the beam-spot size, D_l is definitely far too small compared to what is expected for micellar aggregates whose hydrodynamics radius is of the order of 10 nm.

The former 'double relaxation' behaviour occurs only in a very narrow temperature range (of the order of a couple of degrees) around T^*. The inset in Fig. 6, however, shows that mass diffusion displays an unexpected reduction over the whole micellization region and for all the investigated concentration values. In fact, even for a P407 dilute solution at 1% w/w the minimum value of D, which occurs for a temperature close to the value where S_T is minimal, is about 4–5 times smaller than at temperatures where micellization has completed. As a consequence of the small values of D, the thermophoretic mobility $D_T = DS_T$, shown in the body of Fig. 6, is consistently quenched in the micellization region. Namely, like the Soret coefficient it is of course negative, but its absolute values are much smaller than at low and high temperature, where the solution is expected to be fully structured into simple unimers or micelles respectively. It is also worth noticing that the values of D_T at temperatures that are just below and just above the micellization region are pretty similar, regardless of this consistent structural change, similarly to what happens in the micellization of simple surfactants.[50]

6.2 DLS correlation functions

The anomalous 'slowing down' of the apparent diffusion coefficient within the micellization region opens up several questions about the physical mechanism leading to the buildup of the

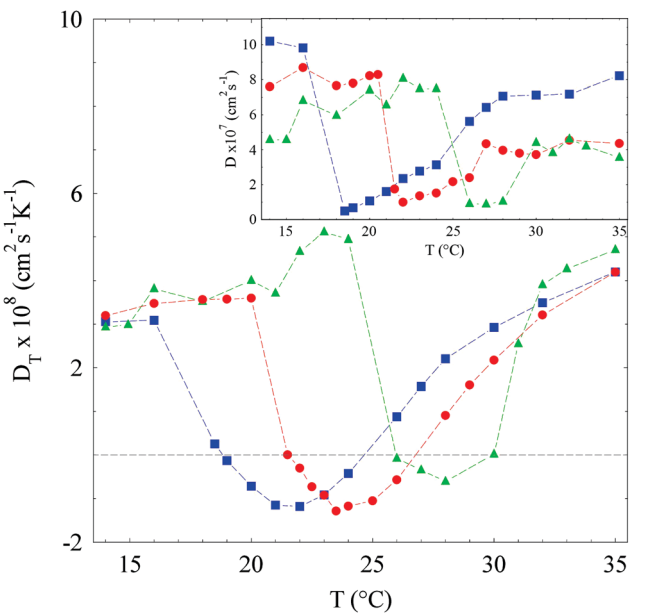

Fig. 6 Inset: Temperature dependence of the diffusion coefficient D for P407 solutions at 1% (triangles), 5% (circles) and 10% (squares) weight fraction. For the narrow regions around T^* where $\vartheta_S(t)$ displays a double relaxation, we took $D = D_l$. The thermophoretic mobility $D_T = S_T D_T$ is shown in the figure body with the same symbols.

thermally-induced concentration gradient. It is then advisable to compare the results derived from TL measurements with those obtained by other methods, the natural choice being of course DLS. Unfortunately, early studies of P407 by DLS were either limited to temperatures where micellization has fully taken place[53] or just tried to reconstruct the distribution of the aggregate size by using standard regularized Laplace inversion software (CONTIN) that often gives questionable results and, more than that, is not suitable at all to detect nonexponential contributions to the decay of the DLS correlation function deriving from complex collective effects. The only detailed and very accurate DLS study of poloxamer self-association we are aware of was performed on semidilute and concentrated ($c \geq 10\%$ w/w) solutions of Pluronic® F64 ($EO_{78}PO_{30}EO_{78}$).[54] In their study, Nyström and Kjøniksen highlighted a very complex structure of the DLS correlation functions, which were found to behave as a single exponential at short time, showed a pronounced stretched exponential tail at long time, and often displayed a power-law over intermediate timescales. Several of these features, and in particular the occurrence of slow non-exponential relaxation modes whose origin is still debated, are ubiquitous in semidilute polymer solutions, in particular when they approach the transition to a gel phase.[55]

Prompted by the puzzling behaviour of the TL dynamics, we have performed an extensive DLS investigation of P407 as a function of concentration and temperature that will be fully reported elsewhere. For the purposes of this work, however, it is useful to discuss at least the evidence we collected for a dilute solution (c = 1% w/w) of P407, which may in principle be expected to show a much simpler behaviour than the systems investigated by Nyström and Kjøniksen. Rather astonishingly, however, several features observed in semidilute and concentrated solutions are preserved with minor differences. Even more, strong deviations from a 'simple' behaviour of the correlation functions are found exactly where one does not expect them, namely at temperatures well below micellization.

Some DLS field-correlation functions $g_1(t)$ obtained at a scattering angle $\theta = 90^\circ$, corresponding to a scattering wavevector $q \simeq 2.23 \times 10^5$ cm^{-1}, are shown in the inset of Fig. 7. Consider first the correlation function obtained at the lowest investigated temperature, $T = 15$ °C, which evidently shows two distinct time regions. At short time (region 1) $g_1(t)$ decays as a simple exponential with a time constant $\tau_1 \simeq 30$ μs, which yields a diffusion coefficient $D_1 \simeq 7 \times 10^{-7}$ nm, and a hydrodynamic radius $R_H \simeq 3$ nm. Yet, most of the decay of the correlation time is due to a much slower relaxation (region 2), which can be fitted as a slightly compressed exponential $\exp[-(t/\tau_2)^\beta]$, where $\beta \simeq 1.2$ and $\tau_2 \simeq 6.5$ ms.§§ Closer to the cmt ($T \geq 19$ °C), however, the long-time behaviour of $g_1(t)$ switches from a compressed exponential to a power-law (region 3), whose contribution can be fitted as $(1 + t/\tau_3)^{-\gamma}$, where $\gamma \simeq 1/2$. Notably, the decay constant τ_1 of region 1 does not appreciable change,

§§ Due to the strong dependence of the scattered intensity on size, the structure that generates this strong scattering contribution may nevertheless involve a small fraction of the unimers.

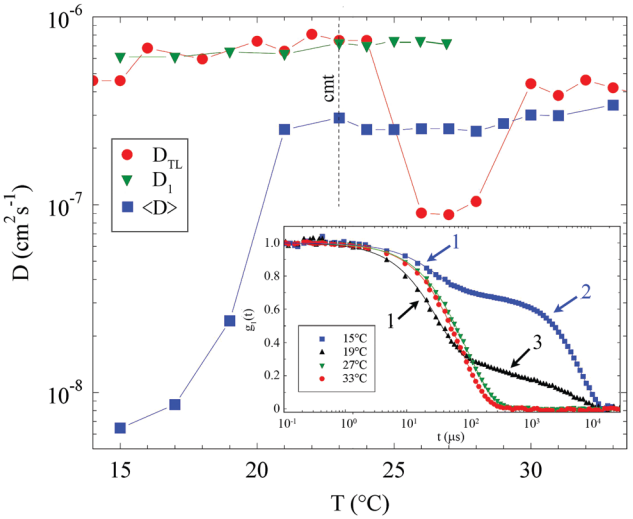

Fig. 7 Inset: DLS correlation functions at $\theta = 90^\circ$ for a 1% P407 solution at several temperatures, highlighting the different time regions discussed in the text. Body: Short time (D_1) and average $\langle D \rangle$ diffusion coefficients obtained by DLS, compared to the values D_{TL} obtained by TL.

suggesting that the short-time contribution is simply due to free unimers. Yet, just above the cmt the power-law tail disappears and the amplitude of the short-time contribution rapidly decreases, becoming too weak to be properly fitted when $T \gtrsim 27$ °C. For higher T, $g_1(t)$ is indeed an almost pure exponential, but with a longer and almost T-independent decay time of about 100 μs corresponding to $R_H \simeq 11$ nm, the size of P407 micelles. Nevertheless, the temperature dependence of the scattered intensity $I_s(T)$, shown in inset A of Fig. 2, indicates that even above 30 °C micellization has not fully completed, suggesting that a non-negligible fraction of the poloxamer is still in unimer form. In fact, by interpolating between the minimum value of $I_s(T)$, obtained at $T \simeq 22$ °C and regarded as the intensity scattered by a solution of unimers, and its asymptotic value for $T \gtrsim 35$ °C, where P407 is fully micellized, one can obtain the temperature dependence of the fraction $f(T)$ of P407 molecules associated into micelles, which is shown in Fig. 8.

Before comparing the DLS correlation functions with the TL transients, let us briefly comment on the peculiar behaviour of the DLS correlation functions below the cmt. As pointed out, the experiments by Nyström and Kjøniksen were performed on semi-dilute or concentrated solutions, where 'slow' relaxation modes are often observed and attributed to the formation of transient, short finite-lifetime networks.[56,57] Our DLS experiments, however, were performed on dilute solutions, far below the polymer overlap concentration c^*, where similar slow modes are not expected. A possible reason why slow diffusive modes can also occur in solutions of poloxamers well below c^* is that, rather than as a Gaussian chain, a unimer may be envisaged as two EO polymer chains joined by a more compact globule composed of the PO groups. Because of the partial hydrophobicity of the latter, these connecting globules may act as 'sticky spots' that favour the formation of transient networks even at low concentration. Notably, transient networks with DLS correlation functions

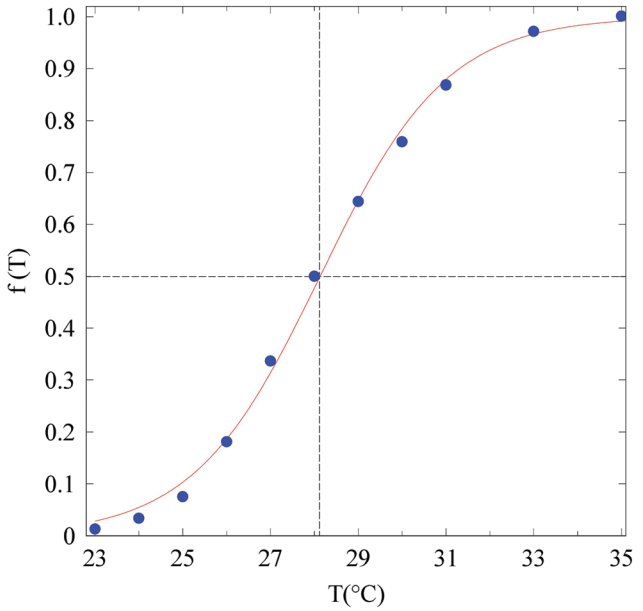

Fig. 8 Temperature dependence of the fraction f of P407 molecules in micellar form, obtained from the data in inset A of Fig. 2 as described in the text. The full line is a tentative fit to the data with the function $f(T) = (1/2)\{\tanh[\pi(T - T_0)/\Delta T] + 1\}$, where $T_0 \simeq 28$ °C is the temperature at which half of the unimers have associated into micelles, and $\Delta T \simeq 9$ °C is the temperature range over which f varies by 90%.

displaying one or more slow relaxation modes have recently been observed in dilute solutions of telechelic tri-block copolymers with a soluble middle block and two associating end units.[58] This tentative explanation requires of course to be supported by further evidence.

6.3 TL dynamics *versus* DLS

Contrasting the time-dependence of the TL signals with the Brownian dynamics probed by DLS requires one to properly define one or more characteristic decay times of the correlation functions. However, while for $T \leq 27$ °C the initial decay of $g_1(t)$ yields a well-defined short-time diffusion coefficient $D_1 = (q^2\tau_1)^{-1}$, quantifying the long-time dynamics is harder because of the complex and T-dependent shape of the correlation functions. Therefore, as commonly done when dealing with complex DLS relaxations, we shall gauge the overall behaviour of $g_1(t)$ by introducing an average diffusion coefficient $D = (q^2\tau)^{-1}$, where τ is the time-integral of the correlation function,

$$\tau = \int_0^\infty g_1(t)\mathrm{d}t, \tag{17}$$

which, when $g_1(t)$ is a simple exponential, coincides of course with its decay time. The evidence presented in Fig. 7, where the diffusion coefficients D_{TL} obtained from the TL measurements are compared with both D_1 and D, can be summarized as follows:

• For $T \leq 23$ °C, the nominal cmt of P407 at 1% w/w, D_{TL} basically coincides with D_1, indicating the presence of unimers with a hydrodynamic radius $R_H \simeq 3$ nm. The reason why the contribution with a much slower decay time that we tentatively attributed to the presence of a transient network is not seen in TL measurements is arguably due to the very different timescales probed by the two techniques. Indeed, while DLS probes diffusion on timescales of the order of $(\langle D\rangle q^2)^{-1}$, which in our case does not exceeded tens of milliseconds, reaching the steady-state in TL measurements requires a much longer time even for the free P407 unimers. Hence, if the transient network has a much shorter lifetime than its diffusion time over the beam-spot size, it will not contribute to the buildup of the TL signal.

• In the micellization region 23 °C $\leq T \leq$ 29 °C, D_{TL} displays a drop by almost one order of magnitude. This slowing down of diffusion in thermophoresis is not observed in DLS measurements, which conversely, in agreement with the behaviour of $I_s(t)$, show the contemporary presence of micelles with a radius $R_H \simeq 11$ nm in equilibrium with a rapidly decreasing fraction of free unimers.

• For $T \geq 30$ °C, D_{TL} becomes comparable with (actually 20–30% larger than) $\langle D\rangle$, namely with the diffusion constant of the P407 micelles. Hence, when micellization has completed, TL and DLS basically probe the same microscopic dynamics.

7 Discussion

The unexpected behaviour of thermophoresis in the P407 micellization region requires at least a tentative explanation. As a matter of fact, from the values of $S_T > 0$ and $D_T > 0$ at low and high T, we can safely conclude that both unimers and micelles display a thermophilic behaviour: why then should a mixture of unimers and micelles move to the hot side? We believe that this rather puzzling inversion of thermophoretic motion may be accounted for by observing that the poloxamer solution in the micellization region is a mixture of unimers and micelles with a temperature-dependent equilibrium composition, which therefore varies along the steady-state profile.

Let us indeed call f, as in Fig. 8, the fraction of molecules that are incorporated into micelles at temperature T, so that the total weight fractions of micellized P407 and of unimers are respectively given by fc and $(1 - f)c$. Hence, by calling D^1 and D^m the diffusion coefficients of, respectively, unimers and micelles, and D_T^1 and D_T^m the corresponding thermophoretic mobilities, for $c \ll 1$ the total mass flux J can be written

$$J = -D^m\nabla(fc) - D^1\nabla[(1 - f)c] - c[fD_T^m + (1 - f)D_T^1]\nabla T.$$

If we define a weight-averaged diffusion coefficient and thermophoretic mobility as

$$\begin{cases} \langle D\rangle = fD^m + (1 - f)D^1 \\ \langle D_T\rangle = fD_T^m + (1 - f)D_T^1, \end{cases} \tag{18}$$

we must then have at steady state ($J = 0$)

$$\langle D\rangle\nabla c - c(D^1 - D^m)\nabla f = -c\langle D_T\rangle\nabla T,$$

which shows that the steady-state concentration gradient,

$$\nabla c = -c\frac{\langle D_T\rangle\nabla T - (D^1 - D^m)\nabla f}{\langle D\rangle},$$

is explicitly dependent on the spatial gradient of the fraction of micellized poloxamer multiplied by the difference $\Delta D = D^1 - D^m$ between the unimer and micelle diffusion constants. The previous expression can conveniently be re-written as

$$\nabla c = -c\frac{D_T^*}{\langle D\rangle}\nabla T = -cS_T^*\nabla T, \qquad (19)$$

where

$$D_T^* = \langle D_T\rangle - \Delta D\frac{\mathrm{d}f}{\mathrm{d}T} \qquad (20)$$

and $S_T^* = D_T^*/\langle D\rangle$. Eqn (20) shows that the thermophoretic mobility and the Soret coefficient are modified by a term proportional to the temperature derivative of $f(T)$. Besides, since both ΔD and $\mathrm{d}f/\mathrm{d}T$ are positive quantities (see Fig. 8), the latter is a thermophilic contribution that tends to accumulate micelles towards the (warmer) beam center, consistently with the temperature dependence of the equilibrium partition between unimers and micelles. In addition to the usual 'thermal' force[9] $F_T = -k_B T S_T \nabla T$ we then have a further effective force $F_\mu = k_B T(\Delta D/\langle D\rangle)\nabla f$ that, in the absence of thermophoresis, would generate the concentration profile required by local equilibrium of the chemical potentials of the two species. Notice that F_T acts against this 'chemical' force. In fact, because of the contribution of F_μ, the (apparent) thermophoretic mobility would, in the absence of F_T, be negative through the whole cmt region and basically zero outside it (besides, its magnitude would be much larger). Once again, this makes it hard to believe that thermophoresis can be consistently obtained from local equilibrium considerations.

For a quantitative test of the model, we took for the unimer and the micelle thermophoretic mobility the roughly equal values $D_T^1 \simeq D_T^m \simeq 5 \times 10^{-8}$ cm^2 s^{-1} K^{-1} (see Fig. 6), for the unimer and micelle diffusion coefficients the values $D^1 = D_s \simeq 6.9 \times 10^{-7}$ cm^2 s^{-1} and $D^m = \langle D\rangle \simeq 2.5 \times 10^{-7}$ cm^2 s^{-1} obtained by DLS just above the cmt (which can be safely attributed to the P407 unimers and micelles), and for the fraction of micellized poloxamer $f(T)$ the data in Fig. 8.

Fig. 9 shows that the theoretical results obtained from eqn (20) agree more than qualitatively with the experimental data for D_T and S_T. Yet, some of the experimental evidence this simple model cannot surely account for is the anomalous decrease of D in the micellization region: as a matter of fact, $\langle D\rangle$ cannot indeed be smaller than D^m. This discrepancy (which would arguably be more pronounced for the measurements performed at higher P407 concentration) arises from an implicit assumption we made, namely that the local unimer-micelle equilibrium is reached on very short timescales, so that the time-evolution of the concentration profile is fully ruled by the diffusion of the two coexisting species. The TL dynamics seems therefore to question this assumption, which is nevertheless supported by T-jump experiments.[59] We do not have so far any plausible explanation for this discrepancy.

Summing up, we hope we have convinced the reader that the investigation of thermophoretic effects grants novel and complementary evidence about the complex self-association processes taking place in aqueous solutions of amphiphilic block copolymers. More generally, we regard the approach we followed as very promising for the investigation of thermal forces in other systems displaying a temperature-dependent equilibrium between coexisting chemical species or states of aggregation, such us for instance proteins undergoing oligomerization by changing T. As a further bonus, we have shown that the optothermal excitation method exploited in TL also provides direct information on thermal properties of disperse systems such as the thermal expansivity, which allows one for instance to highlight compaction effects upon micellization. Therefore, we regard the application of TL to other self-association processes as a very interesting and stimulating prospect.

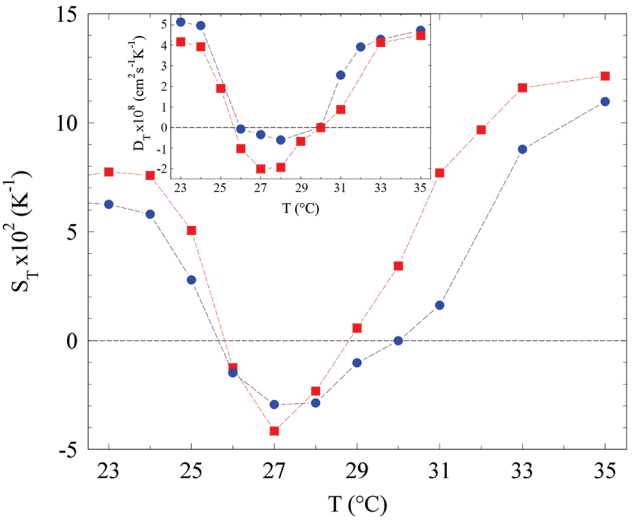

Fig. 9 Inset: Comparison of the results for the experimental data for the thermophoretic mobility D_T of a P407 solution at 1% w/w (bullets) with the theoretical values obtained from eqn (20) (squares). The figure body shows, with the same symbols, the comparison between S_T and S_T^*, obtained as D_T^*/D.

Conflicts of interest

There are no conflicts to declare.

Acknowledgements

We thank M. Stefanoni for help with preliminary measurements and L. Cipelletti for interesting suggestions.

References

1 J. V. Tyrrell, *Diffusion and Heat Flow in Liquids*, Buttherworths, London, 1961.
2 S. R. D. Groot and P. Mazur, *Nonequilibrium thermodynamics*, North Holland, Amsterdam, 1962.
3 S. Sasa and H. Tasaki, *J. Stat. Phys.*, 2006, **125**, 125.
4 E. H. Kennard, *Kinetic Theory of Gases*, McGraw-Hill, New York, 1938.

5 L. van't Hoff, *Philos. Mag. S5*, 1888, **26**, 81.
6 R. Ganti, Y. Liu and D. Frenkel, *Phys. Rev. Lett.*, 2017, **119**, 038002.
7 R. Ganti, Y. Liu and D. Frenkel, *Phys. Rev. Lett.*, 2018, **121**, 068002.
8 S. Wiegand, *J. Phys.: Condens. Matter*, 2004, **16**, R357.
9 R. Piazza and A. Parola, *J. Phys.: Condens. Matter*, 2008, **20**, 153102.
10 J. L. Anderson, *Annu. Rev. Fluid Mech.*, 1989, **21**, 61.
11 A. Parola and R. Piazza, *Eur. Phys. J. E: Soft Matter Biol. Phys.*, 2004, **15**, 255.
12 A. Würger, *Rep. Prog. Phys.*, 2010, **73**, 126601.
13 S. Iacopini, R. Rusconi and R. Piazza, *Eur. Phys. J. E: Soft Matter Biol. Phys.*, 2006, **19**, 59.
14 Y. Kishikawa, *et al.*, *Phys. Chem. Chem. Phys.*, 2012, **14**, 10147.
15 A. Cuche, *et al.*, *Nano Lett.*, 2013, **13**, 4230.
16 J. Chen, *et al.*, *Sci. Rep.*, 2016, **6**, 35814.
17 H. Cong, J. Chen and H. Ho, *Sens. Actuators, B*, 2018, **264**, 224.
18 P. F. Geelhoed, R. H. Lindken and J. Westerweel, *Chem. Eng. Res. Des.*, 2006, **84**, 1.
19 D. Vigolo, R. Rusconi, H. A. Stone and R. Piazza, *Soft Matter*, 2010, **6**, 3489.
20 C. J. Wienken, P. Baaske, U. Rothbauer, D. Braun and S. Stefan, *Nat. Commun.*, 2010, **1**, 100.
21 S. Seidel, *et al.*, *Methods*, 2006, **59**, 301.
22 M. R. Reichl and D. Braun, *J. Am. Chem. Soc.*, 2014, **136**, 15955.
23 J. P. Gordon, R. C. C. Leite, R. S. Moore, S. P. S. Porto and J. R. Whinnery, *J. Appl. Phys.*, 1965, **36**, 3.
24 J. R. Whinnery, D. T. Miller and F. Dabby, *IEEE J. Quantum Electron.*, 1967, **3**, 382.
25 C. A. Carter and J. M. Harris, *Appl. Opt.*, 1984, **23**, 476.
26 R. F. Souza, *et al.*, *J. Phys.: Condens. Matter*, 2008, **20**, 155102.
27 S. E. Bialkowski, *Photothermal Spectroscopy Methods for Chemical Analysis*, Wiley, New York, 1996.
28 M. Franko and C. D. Tran, *Rev. Sci. Instrum.*, 1996, **67**, 1.
29 M. A. Proskurnin, *et al.*, *J. Anal. Chem.*, 2015, **70**, 249.
30 M. Liu and M. Franko, *Int. J. Thermophys.*, 2016, **37**, 67.
31 M. Giglio and A. Vendramini, *Appl. Phys. Lett.*, 1974, **25**, 555.
32 R. Rusconi, L. Isa and R. Piazza, *J. Opt. Soc. Am. B*, 2004, **21**, 605.
33 R. Rusconi, E. Rodari and R. Piazza, *Appl. Phys. Lett.*, 2006, **89**, 261916.
34 R. Rusconi, PhD thesis, Politecnico di Milano, 2007.
35 P. Alexandridis and T. A. Hatton, *Colloids Surf., A*, 1995, **96**, 1.
36 A. M. Bodratti and P. Alexandridis, *J. Funct. Biomater.*, 2018, **9**, 11.
37 D. Bedrov, C. Ayyagari and G. D. Smith, *J. Chem. Theory Comput.*, 2006, **2**, 598.
38 I. Goldmints, J. F. Holzwarth, K. A. Smith and T. A. Hatton, *Langmuir*, 1997, **13**, 6130.
39 G. Wanka, H. Hoffmann and W. Ulbricht, *Macromolecules*, 1994, **27**, 4145.
40 C. Wu, *et al.*, *Macromolecules*, 1997, **30**, 4574.
41 G. Dumortier, J. Grossiord, F. Agnely and J. Chaumeil, *Pharm. Res.*, 2006, **23**, 2709.
42 A. Fakhari, M. Corcoran and A. Schwarz, *Heliyon*, 2017, **3**, e00390.
43 Q. Wang, *et al.*, *Eur. Polym. J.*, 1993, **29**, 1665.
44 M. Bohorquez, C. Koch, T. Trygstad and N. Pandit, *J. Colloid Interface Sci.*, 1999, **216**, 34.
45 K. Mortensen and Y. Talmon, *Macromolecules*, 1995, **28**, 8829.
46 K. Mortensen, *Polym. Adv. Technol.*, 2001, **12**, 2.
47 R. K. Prud'homme, G. Wu and D. K. Schneider, *Langmuir*, 1996, **12**, 4651.
48 M. S. Baptista and C. D. Tran, *J. Phys. Chem.*, 1995, **99**, 12952.
49 T. Liu, V. M. Nace and B. Chu, *Langmuir*, 1999, **15**, 3109.
50 D. Vigolo, S. Buzzaccaro and R. Piazza, *Langmuir*, 2010, **26**, 7792.
51 A. Parola, R. Piazza and V. Degiorgio, *J. Chem. Phys.*, 2014, **141**, 124902.
52 G. Wanka, H. Hoffmann and W. Ulbricht, *Colloid Polym. Sci.*, 1990, **268**, 101.
53 G.-E. Yu, *et al.*, *J. Chem. Soc., Faraday Trans.*, 1992, **88**, 2537.
54 B. Nyström and A. Kjøniksen, *Langmuir*, 1997, **13**, 4520.
55 J. Li, T. Ngai and C. Wu, *Polym. J.*, 2010, **42**, 609.
56 F. Tanaka and S. F. Edwards, *Macromolecules*, 1992, **25**, 1516.
57 M. C. Blanco, D. Leisner, C. Vázquez and M. A. López-Quintela, *Langmuir*, 2000, **16**, 8585.
58 M. Bohdan, J. Sprakel and J. van der Gucht, *Phys. Rev. E*, 2016, **94**, 032507.
59 E. Hecht and H. Hoffmann, *Colloids Surf.*, 1995, **96**, 181.